SCIENCE CHINA Chemistry

Reversed configuration of photocatalyst to exhibit improved properties of basic processes compared to conventional one

Juhong Lian, Yu Qi, Yunfeng Bao, Zixi Yin, Yang Zhang, Nengcong Yang, Naijia Guan, Shengye Jin, Landong Li and Fuxiang Zhang

Citation: SCIENCE CHINA Chemistry **63**, 771 (2020); doi: 10.1007/s11426-020-9752-x

View online: http://engine.scichina.com/doi/10.1007/s11426-020-9752-x

View Table of Contents: http://engine.scichina.com/publisher/scp/journal/SCC/63/6

Published by the Science China Press

SCIENCE CHINA
Chemistry

•COMMUNICATIONS•

June 2020 Vol.63 No.6: 771–776
https://doi.org/10.1007/s11426-020-9752-x

Reversed configuration of photocatalyst to exhibit improved properties of basic processes compared to conventional one

Juhong Lian[1,2], Yu Qi[1], Yunfeng Bao[1], Zixi Yin[3], Yang Zhang[1], Nengcong Yang[1], Naijia Guan[2], Shengye Jin[3], Landong Li[2*] & Fuxiang Zhang[1*]

[1]*State Key Laboratory of Catalysis, iChEM, Dalian Institute of Chemical Physics, Chinese Academy of Sciences, Dalian National Laboratory for Clean Energy, Dalian 116023, China;*
[2]*School of Materials Science and Engineering, National Institute for Advanced Materials, Nankai University, Tianjin 300350, China;*
[3]*State Key Laboratory of Molecular Reaction Dynamics and Collaborative Innovation Center of Chemistry for Energy Materials (iChEM), Dalian Institute of Chemical Physics, Chinese Academy of Sciences, Dalian 116023, China*

Received January 16, 2020; accepted April 20, 2020; published online May 7, 2020

Performances of semiconductor photocatalysts are integrally determined by efficiencies of basic processes such as light absorption, charge separation and surface catalysis, but conventional configurations of photocatalysts normally suffers from the competition of light absorption originating from cocatalyst deposition and limited interface charge separation between the photocatalyst and cocatalyst. Herein we give the first proof-of-concept illustration that a reversed configuration of photocatalysts with a core/shell structure of microsized Mo_2N cocatalysts and nanosized CdS photocatalysts, which exhibits superior solar hydrogen production to the conventional configuration with nanosized Mo_2N cocatalysts deposited on the surface of CdS photocatalysts. It is revealed that the reversed configuration outperforms the conventional one in all areas of light absorption, charge separation and surface catalysis. Strikingly, the special core/shell structure introduced here can well avoid the competition of light absorption by cocatalysts and make an effective confinement effect to promote the surface catalysis of Mo_2N. Our finding provides an alternative strategy to improve performances of photocatalysts.

photocatalyst, nitride, semiconductor, renewable hydrogen, core/shell

Citation: Lian J, Qi Y, Bao Y, Yin Z, Zhang Y, Yang N, Guan N, Jin S, Li L, Zhang F. Reversed configuration of photocatalyst to exhibit improved properties of basic processes compared to conventional one. *Sci China Chem*, 2020, 63: 771–776, https://doi.org/10.1007/s11426-020-9752-x

Hydrogen production using renewable energy has inspired extensive interest since the finding of Fujishima-Honda effect in 1972 [1]. During the past decades, over hundreds of semiconductors have been developed as photocatalysts for promising solar water splitting, but most of them are not active/effective for the surface catalysis to produce hydrogen [2–12]. To address it, noble metals, such as Pt, Rh and Pd, are normally loaded on the surface of semiconductors to act as cocatalysts to promote the surface catalysis [13–17]. Besides the decrease of surface reaction activation barriers/overpotentials, the cocatalyst is also known to favor the transfer and separation of photogenerated electrons from the semiconductors [18,19]. Accordingly, loading the cocatalysts plays a significant role in promoting the photocatalytic water splitting performances, which has become a general strategy in the field of solar water splitting.

Conventionally, the nanoparticles of noble metal cocatalysts have been loaded on the surface of nanosized/microsized semiconductors. However, this configuration generally confronts some shortcomings. For example, the surface-loaded dark-color noble metals will preferentially absorb light, resulting in decreased light absorption efficiency of the

*Corresponding authors (email: lild@nankai.edu.cn; fxzhang@dicp.ac.cn)

semiconductors [20]. On the other hand, the interface contact between cocatalysts and semiconductors is too insufficient to cause efficient charge separation at the interface, in consideration of the facts that the nanosized semiconductor normally suffers from aggregation [21], while the microsized one owns relatively low surface sites exposed and has a long distance of electron transfer within the bulk [22]. Resulting from the competition of light absorption and inefficient charge transfer, the activities of photocatalysts with the conventional configuration (*i.e.*, loading nanosized cocatalysts on the surface of semiconductors) are mostly unsatisfactory. To address above key issues, it is highly desirable to develop a novel configuration of photocatalysts.

It is additionally noting that the noble metal is too expensive to be for hydrogen production at a large scale, even though the loading of noble metals, especially for metallic platinum, exhibited superior performances [23]. To overcome the dependence on noble metals, the development of non-noble metal-based cocatalysts has recently inspired continuous interest [24]. For example, some transition metal-based nitrides [25-27], carbides [28,29] or sulfides [30,31] have been developed as efficient hydrogen evolution electrocatalysts and cocatalysts of photocatalytic systems for the purpose of replacing the noble metals. Unfortunately, the non-noble metals have been also employed as nanosized cocatalysts for the assembly of conventional configurations of photocatalysts.

Herein we introduce a reversed configuration (compared to the conventional one) of photocatalysts fabricated by depositing nanosized CdS (semiconductor) on the surface of microsized Mo_2N hexagonal rods (cocatalyst). The whole structure can be coarsely described as a core/shell structure. The as-obtained reversed photocatalyst is denoted as Mo_2N@CdS. For comparison, the photocatalyst with conventional configurations (called as conventional configuration later) was fabricated by depositing nanosized Mo_2N (cocatalyst) on the surface of bulk CdS (semiconductor), and the corresponding sample is denoted as Mo_2N/CdS. Additionally, the nanosized Pt loaded CdS nanoparticles with conventional configurations was also prepared for extended discussion, which is denoted as Pt/CdS. Based on their corresponding optimization, the H_2 evolution rate on the Mo_2N@CdS sample under visible light irradiation is remarkably superior to that of Mo_2N/CdS or Pt/CdS. According to our detailed characterizations and discussion, the superior photocatalytic H_2 evolution rate of the Mo_2N@CdS sample is mainly attributed to its special advantages in all the areas of light absorption, charge separation and surface catalysis: 1) the core/shell structure in the reversed configuration can ensure the preferential light absorption of the CdS semiconductor to even avoid the competition of light harvesting caused by the Mo_2N cocatalyst; 2) much better charge separation is observed for the reversed configuration with respect to the conventional ones; 3) the core/shell structure makes an effective confinement effect to promote the surface catalysis of Mo_2N.

As seen in the illustration of Figure 1(a), the Mo_2N@CdS photocatalyst was basically constructed by three steps. First of all, the MoO_3 hexagonal rods were prepared by an oil bath method. Secondly, the MoO_3 hexagonal rods were employed as precursors to prepare Mo_2N hexagonal rods under the flow of ammonia. Finally, the microsized Mo_2N hexagonal rods were employed as cocatalysts, and on the surface a calculated amount of CdS was deposited by a simple hydrothermal process to obtain the reversed core/shell configuration. The detailed experimental procedure is illustrated in the Experimental section. If not specially stated, the samples denoted as Mo_2N@CdS, Mo_2N/CdS and Pt/CdS stand for those with optimized content of cocatalysts, respectively.

As given in Figure 1(b), a single phase of MoO_3 and Mo_2N can be confirmed according to the observation that all the X-ray diffraction peaks are well indexed to the hexagonal phase of MoO_3 (PDF# 21-0569) and the cubic phase of Mo_2N (PDF# 25-1366), respectively. After depositing CdS on the surface of Mo_2N, the diffraction peaks attributed to the Mo_2N phase are well kept, accompanying with the diffraction peaks of hexagonal phases of CdS (PDF# 41-1049). This demonstrates the good composite of both Mo_2N and CdS by the experimental procedure. The hexagonal MoO_3 and Mo_2N rods can be separately observed in Figure 1(c, d). Intriguingly, the Mo_2N rods with the length of 5–15 μm are well dispersed free of aggregation. Additionally, the CdS nano-

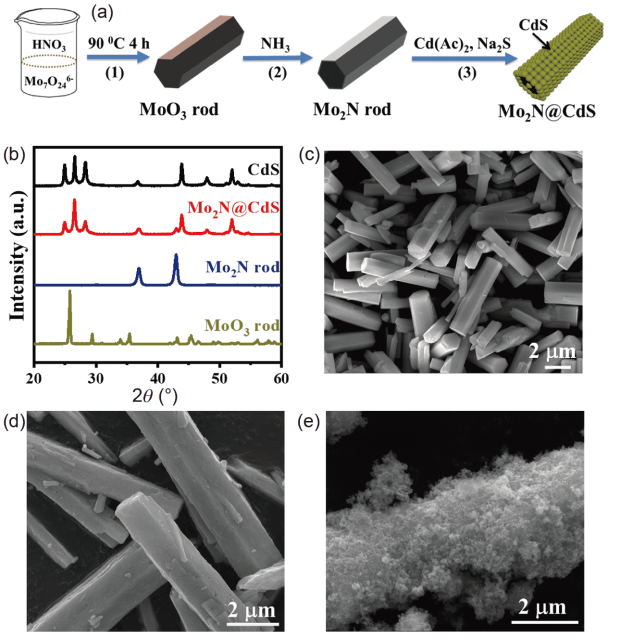

Figure 1 (a) An illustration on the preparation of Mo_2N@CdS core-shell structures. (b) XRD patterns of the MoO_3 hexagonal rods, Mo_2N hexagonal rods, Mo_2N@CdS and CdS samples. SEM images of the MoO_3 hexagonal rods (c), Mo_2N hexagonal rods (d) and Mo_2N@CdS core-shell structures (e) (color online).

particles with the particle size of *ca.* 30–50 nm are mainly dispersed around the Mo_2N hexagonal rods (Figure 1(e)) to form the reversed core/shell structure. High resolution scanning electron microscopy (HRSEM, see Figure S2, Supporting Information online) images more clearly show that CdS nanoparticles grow on the surface of Mo_2N rods uniformly. The SEM image of pristine CdS in Figure S1 shows an aggregated morphology with the particle sizes of 30–50 nm. The typical structures and morphologies of the Pt/CdS and Mo_2N/CdS samples are given in Figures S3–S5, respectively. As expected, the diffraction peaks assigned to the deposited Pt or Mo_2N nanoparticles are not observed, demonstrating their small size and/or amorphous structures. However, obvious aggregation of the Mo_2N nanoparticles on the surface of bulk CdS can be observed (Figure S4). The Pt nanoparticles by the photodeposition method can be also observed on the surface of CdS (Figure S5).

Photocatalytic H_2 evolution rates were evaluated in the aqueous solution containing lactic acid (as hole scavengers) under visible light irradiation. All the samples show no obvious H_2 evolution under dark condition, and no obvious H_2 was detected for the pure Mo_2N hexagonal rod under visible light, either. The CdS shows a low H_2 evolution rate (*ca.* 45 μmol/h). This means that CdS can act as photocatalysts for the H_2 evolution, and the Mo_2N can only work as cocatalysts. The dependence of content of cocatalysts on the initial H_2 evolution rate was first optimized (Figure S6). Figure 2(a) gives their typical time courses of H_2 evolution on the optimized samples, in which the amount of generated H_2 almost linearly increased after 1 h induced irradiation, demonstrating their good photochemical stability in the experimental region. Figure 2(b) further compares their optimal average activities, based on which the Mo_2N@CdS sample exhibits remarkably superior performance with respect to the Pt/CdS or Mo_2N/CdS samples. To evaluate the stability of reversed Mo_2N@CdS core/shell structures, the XRD patterns of Mo_2N@CdS were measured after the photocatalytic H_2 evolution reaction. As shown in Figure S7, no obvious changes of XRD patterns were observed before and after the photocatalytic reaction, demonstrating that the Mo_2N@CdS core/shell structure is stable under the experimental conditions.

In order to get insight into the superior performance of the reversed configuration with respect to the conventional ones, the typical three samples are thus analyzed and compared in detail. Firstly, their charge separation performances were analyzed and compared by measuring their steady-state photoluminescence (PL), time-resolved photoluminescence (TRPL) spectra, transient photocurrent response and electrochemical impedance spectra (EIS). As demonstrated by the PL results in Figure 3(a), all the samples show the fluorescence signals at 525 nm due to intrinsic band-band transitions while the much lower PL intensity of Mo_2-

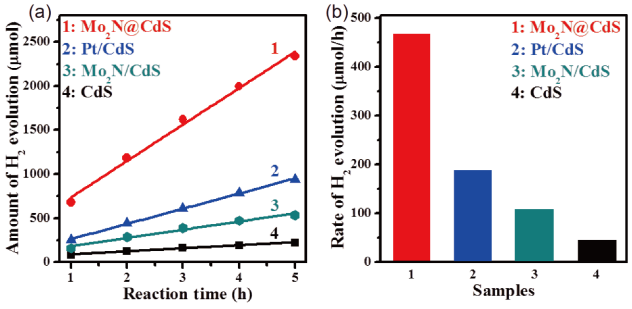

Figure 2 Comparison of the photocatalytic H_2 evolution performance on typical samples. (a) Time courses of H_2 evolution; (b) the average H_2 generation rate. Reaction conditions: 20 mg CdS; 100 mL, 10 vol% lactic acid aqueous solution; 300 W xenon lamp ($\lambda \geqslant 420$ nm); reaction time: 5 h (color online).

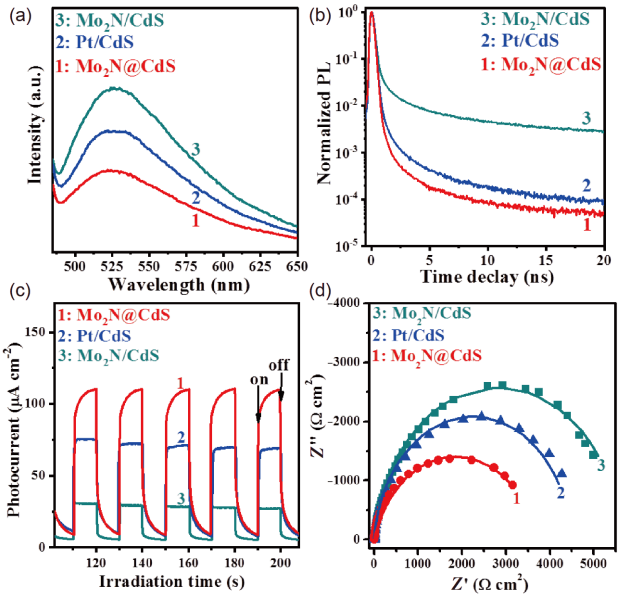

Figure 3 The charge separation performance of the typical three samples. (a) Steady PL spectra; (b) TRPL decay spectra; (c) transient photocurrent responses recorded at the potential of 0.9 V *vs.* RHE in 0.5 M Na_2S and 0.5 M Na_2SO_3; (d) Nyquist plots tested at 0.9 V *vs.* RHE; frequency: 0.1 Hz–10 kHz (color online).

N@CdS than the other two samples is observed, indicating that the reversed Mo_2N@CdS shows more effective charge separation between CdS and Mo_2N cocatalysts than the other two samples. TRPL spectra were further performed to measure the charge separation dynamics. The cocatalysts can accept the photogenerated electrons from excited photocatalysts to allow additional nonradiative decay channels, and decrease the fluorescence lifetime [32–36]. As shown in Figure 3(b), Mo_2N@CdS displays the fastest PL decay lifetime, which implies that the efficient contact interface of reserved Mo_2N@CdS configurations can accelerate the electrons transfer from CdS to Mo_2N compared to the conventional configuration samples. The superior charge separation between photocatalysts and cocatalysts will lead to excellent photoelectrocatalytic performances. Expectedly,

transient photocurrent results reveal that reserved Mo_2N@CdS exhibits enhanced photocurrent responses compared with Pt/CdS or Mo_2N/CdS samples (Figure 3(c)), suggesting that this reserved Mo_2N@CdS can promote the separation and transfer of photogenerated electron-hole pairs. The current enhancement and decay during the light-on and -off period may result from the charge and discharge of the sample [37]. Meanwhile, the Mo_2N@CdS shows much smaller electrolyte interface charge transfer resistance (R_{ct}) than that of Pt/CdS or Mo_2N/CdS, further demonstrating better charge separation and transfer of the Mo_2N@CdS (Figure 3(d)). It is worth noting that trends of the intensity of PL spectra, TRPL decay lifetime, transient photocurrent responses and the charge transfer resistance on the three typical samples are all in good accordance with their activity order. This demonstrates that the charge separation plays a remarkable role in determining their activities.

Encouraged by the superior charge separation performance on the reversed configuration, we continuously investigated the feature of surface catalysis and light harvesting in the Mo_2N@CdS sample. As seen in Figure 4(a), the Mo_2N rods show the effective electrocatalytic water reduction, confirming its function of cocatalysts for the H_2 evolution. Intriguingly, the electrocatalytic performance of Mo_2N rods is remarkably promoted after the deposition of CdS which is not active for the water reduction at all. This means that a nano-confined effect may result from the special core/shell structure. The nano-confined effect can be explained by electron interactions and stack porous structure of CdS nanoparticles. Firstly, the XPS result in Figure 4(b) shows that the binding energy of Mo–N has an obvious negative shift (228.0 eV) after the deposition of CdS nanolayers compared with the pristine Mo_2N rods (228.7 eV), suggesting a strong electron interaction between Mo_2N and CdS in the reversed configuration. The strong electron interactions play an important role in promoting the electrochemical hydrogen production, which benefits to the activation of H_2O [38]. The survey spectrum shows the existence of Cd, S, Mo, N and O elements in Figure S8. In addition, the porous structure originating from the stack of CdS nanoparticles can be formed, in which the H_2O molecules could stay longer and have more opportunities to collide with the Mo_2N surface. The obvious electron exchange and the porous structures are the basic features of nano-confined effect [39–43]. This is consistent with previous reports which the pore-confined space makes a significant promotion effect on the electrochemical efficiency [44,45]. Additionally, the reversed configuration of Mo_2N@CdS shows weaker characteristic absorption of Mo_2N than conventional configurations of Mo_2N/CdS (Figure S9). In order to further analyze the thickness of CdS on the light absorption, CdS films with different thickness were prepared and characterized. As given in Figure 4(c), the transmittance of solar light is strongly dependent on the thickness of CdS layers, and almost complete light absorption before absorption edge can be obtained when the thickness of CdS layers is beyond 350 nm. This means that the competition of light absorption originating from the Mo_2N cocatalyst will be completely avoided once the thickness of CdS shell photocatalysts is over 350 nm.

It has been widely known that the activity of one photocatalyst is integrally determined by the efficiencies of light absorption, charge separation and surface catalysis [46]. On the basis of our above analysis and discussion, the photocatalyst with reversed configurations (*i.e.*, Mo_2N@CdS) is not only favorable for the charge separation but also for the surface catalysis due to the unexpected nano-confined effect. Additionally, the reversed configuration can effectively avoid the competition of light absorption resulting from the cocatalyst, while this is impossible for the conventional configuration. To further illustrate the influence of light absorption competition, we compared a series of reversed photocatalysts with different thicknesses of CdS by adjusting the mass ratio of CdS to Mo_2N rods. As given in Figure S6 (a), the photocatalytic activities of Mo_2N@CdS undergo first increase and subsequent decrease, revealing that the photocatalytic activity is really related to the light absorption ef-

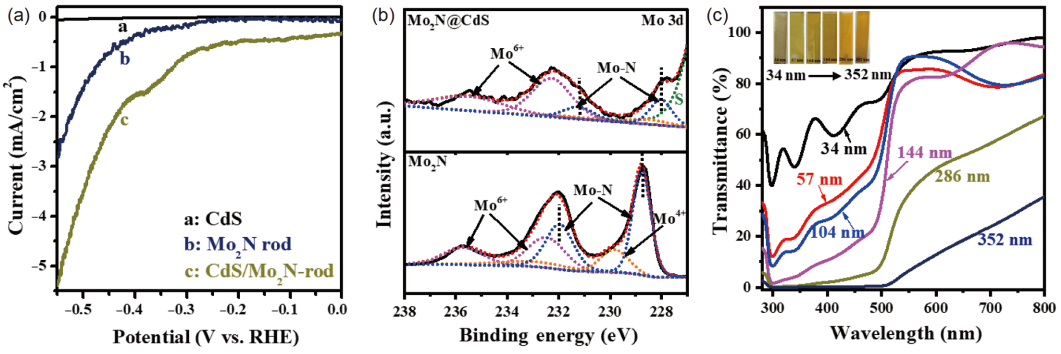

Figure 4 The performances of surface catalysis and light absorption of the Mo_2N@CdS. (a) Current density curves as a function of the applied potential of the CdS, Mo_2N rod and CdS/Mo_2N-rod samples; (b) high-resolution XPS spectra of Mo 3d for Mo_2N rods and Mo_2N@CdS samples; (c) UV-Vis transmittance spectra of CdS films on FTO (color online).

ficiency, and the thickness of the CdS photocatalyst with saturated light absorption should be favorable. Additionally, it is reasonable to deduce that the increasing thickness of CdS layers (*i.e.*, increasing the mass ratio of CdS to Mo_2N) not only favors the light absorption but also simultaneously causes much longer charge transfer distance to render the charge separation more difficult. As an integral effect of light absorption and charge separation, the optimal mass ratio of CdS to Mo_2N is thus observed. In this work, the CdS thickness on the sample with the optimal activity was examined by TEM images (Figure S10), and the average thickness of CdS shells is about 370 nm that is beyond the thickness with the complete light absorption before the absorption of CdS films (350 nm, Figure 4(c)). In this case, the competition of light absorption caused by the Mo_2N cocatalysts is well avoided.

Summarily, we designed and realized an unconventional reversed configuration of photocatalysts using microsized Mo_2N (noble metal free) rods as cocatalyst cores and nanosized CdS as model semiconductor photocatalyst shells, which first exhibit superior solar hydrogen production performances with respect to conventional configurations. The reversed core/shell structure not only favors the charge separation, but also efficiently avoids the competition of light harvesting caused by the loaded cocatalysts and makes an unexpected confinement effect for the better catalysis of water reduction. Integrated by the synergistic promotion of light absorption, charge separation and surface catalysis, the photocatalytic performance of the reversed configuration is obviously superior to that of the conventional ones, which is even higher than that of the noble Pt loaded CdS with conventional configurations. This work gives a proof-of-concept illustration on the potential advantages of reversed configurations introduced here, which may be extended into the fabrication of other reversed nanocomposites with inner 1D (or 2D) cocatalysts and outer 0D photocatalysts to promote solar-to-chemical conversion.

Acknowledgements This work was supported by the National Natural Science Foundation of China (21633009, 21925206); the Dalian National Laboratory For Clean Energy (DNL) Cooperation Fund, Chinese Academy of Sciences (DNL 201913), International Partnership Program of Chinese Academy of Sciences (121421KYSB20190025) and the DICP foundation of innovative research (DICP I201927). F. Zhang thanks the support from Liaoning Revitalization Talents Program (XLYC1807241).

Conflict of interest The authors declare that they have no conflict of interest.

Supporting information The supporting information is available online at http://chem.scichina.com and http://link.springer.com/journal/11426. The supporting materials are published as submitted, without typesetting or editing. The responsibility for scientific accuracy and content remains entirely with the authors.

1 Fujishima A, Honda K. *Nature*, 1972, 238: 37–38
2 Li Q, Guo B, Yu J, Ran J, Zhang B, Yan H, Gong JR. *J Am Chem Soc*, 2011, 133: 10878–10884
3 Hitoki G, Ishikawa A, Takata T, Kondo JN, Hara M, Domen K. *Chem Lett*, 2002, 31: 736–737
4 Chen S, Shen S, Liu G, Qi Y, Zhang F, Li C. *Angew Chem Int Ed*, 2015, 54: 3047–3051
5 Chen S, Qi Y, Ding Q, Li Z, Cui J, Zhang F, Li C. *J Catal*, 2016, 339: 77–83
6 Zheng D, Cao XN, Wang X. *Angew Chem Int Ed*, 2016, 55: 11512–11516
7 Hitoki G, Takata T, Kondo JN, Hara M, Kobayashi H, Domen K. *Chem Commun*, 2002, 1698–1699
8 Maeda K, Terashima H, Kase K, Higashi M, Tabata M, Domen K. *BCSJ*, 2008, 81: 927–937
9 Kailasam K, Schmidt J, Bildirir H, Zhang G, Blechert S, Wang X, Thomas A. *Macromol Rapid Commun*, 2013, 34: 1008–1013
10 Kiss B, Didier C, Johnson T, Manning TD, Dyer MS, Cowan AJ, Claridge JB, Darwent JR, Rosseinsky MJ. *Angew Chem Int Ed*, 2014, 53: 14480–14484
11 Liu GL, Chen CC, Ji HW, Ma WH, Zhao JC. *Sci China Chem*, 2012, 55: 1953–1958
12 Ling X, Xu Y, Wu S, Liu M, Yang P, Qiu C, Zhang G, Zhou H, Su C. *Sci China Chem*, 2020, 63: 386–392
13 Schweinberger FF, Berr MJ, Döblinger M, Wolff C, Sanwald KE, Crampton AS, Ridge CJ, Jäckel F, Feldmann J, Tschurl M, Heiz U. *J Am Chem Soc*, 2013, 135: 13262–13265
14 Dukovic G, Merkle MG, Nelson JH, Hughes SM, Alivisatos AP. *Adv Mater*, 2008, 20: 4306–4311
15 Li Z, Zhang F, Han J, Zhu J, Li M, Zhang B, Fan W, Lu J, Li C. *Catal Lett*, 2018, 148: 933–939
16 Maeda K, Teramura K, Domen K. *J Catal*, 2008, 254: 198–204
17 Wen B, Ma JH, Chen CC, Ma WH, Zhu HY, Zhao JC. *Sci China Chem*, 2011, 54: 887–897
18 Wang Q, Hisatomi T, Jia Q, Tokudome H, Zhong M, Wang C, Pan Z, Takata T, Nakabayashi M, Shibata N, Li Y, Sharp ID, Kudo A, Yamada T, Domen K. *Nat Mater*, 2016, 15: 611–615
19 Yang J, Wang D, Han H, Li C. *Acc Chem Res*, 2013, 46: 1900–1909
20 Ran J, Gao G, Li FT, Ma TY, Du A, Qiao SZ. *Nat Commun*, 2017, 8: 13907
21 Wang D, Li X, Zheng LL, Qin LM, Li S, Ye P, Li Y, Zou JP. *Nanoscale*, 2018, 10: 19509–19516
22 Xiao M, Luo B, Lyu M, Wang S, Wang L. *Adv Energy Mater*, 2018, 8: 1701605
23 Yan H, Yang J, Ma G, Wu G, Zong X, Lei Z, Shi J, Li C. *J Catal*, 2009, 266: 165–168
24 Shi Y, Zhang B. *Chem Soc Rev*, 2016, 45: 1529–1541
25 Shi X, Wu A, Yan H, Zhang L, Tian C, Wang L, Fu H. *J Mater Chem A*, 2018, 6: 20100–20109
26 Yan H, Xie Y, Jiao Y, Wu A, Tian C, Zhang X, Wang L, Fu H. *Adv Mater*, 2018, 30: 1704156
27 Zhu Y, Chen G, Xu X, Yang G, Liu M, Shao Z. *ACS Catal*, 2017, 7: 3540–3547
28 Chen YY, Zhang Y, Jiang WJ, Zhang X, Dai Z, Wan LJ, Hu JS. *ACS Nano*, 2016, 10: 8851–8860
29 Wang S, Wang J, Zhu M, Bao X, Xiao B, Su D, Li H, Wang Y. *J Am Chem Soc*, 2015, 137: 15753–15759
30 Li Y, Wang H, Xie L, Liang Y, Hong G, Dai H. *J Am Chem Soc*, 2011, 133: 7296–7299
31 Jaramillo TF, Jørgensen KP, Bonde J, Nielsen JH, Horch S, Chorkendorff I. *Science*, 2007, 317: 100–102
32 Tu W, Li Y, Kuai L, Zhou Y, Xu Q, Li H, Wang X, Xiao M, Zou Z. *Nanoscale*, 2017, 9: 9065–9070
33 Wang W, Zhu S, Cao Y, Tao Y, Li X, Pan D, Phillips DL, Zhang D, Chen M, Li G, Li H. *Adv Funct Mater*, 2019, 29: 1901958
34 Shi H, Long S, Hu S, Hou J, Ni W, Song C, Li K, Gurzadyan GG, Guo X. *Appl Catal B-Environ*, 2019, 245: 760–769

35 Chen H, Sun Z, Ye S, Lu D, Du P. *J Mater Chem A*, 2015, 3: 15729–15737
36 Zhang H, Lin J, Li Z, Li T, Jia X, Wu XL, Hu S, Lin H, Chen J, Zhu J. *Catal Sci Technol*, 2019, 9: 502–508
37 Liu G, Shi J, Zhang F, Chen Z, Han J, Ding C, Chen S, Wang Z, Han H, Li C. *Angew Chem Int Ed*, 2014, 53: 7295–7299
38 Wang B, Huang H, Huang M, Yan P, Isimjan TT, Yang X. *Sci China Chem*, 2020, https://doi.org/10.1007/s11426-019-9721-0
39 Fu Q, Bao X. *Nat Catal*, 2019, 2: 834–836
40 Wang T, Gao L, Hou J, Herou SJA, Griffiths JT, Li W, Dong J, Gao S, Titirici MM, Kumar RV, Cheetham AK, Bao X, Fu Q, Smoukov SK. *Nat Commun*, 2019, 10: 1340–1348
41 Wang Y, Mao J, Meng X, Yu L, Deng D, Bao X. *Chem Rev*, 2019, 119: 1806–1854
42 Cui T, Dong J, Pan X, Yu T, Fu Q, Bao X. *J Energy Chem*, 2019, 28: 123–127
43 Li H, Guo C, Fu Q, Xiao J. *J Phys Chem Lett*, 2019, 10: 533–539
44 Bae JH, Han JH, Chung TD. *Phys Chem Chem Phys*, 2012, 14: 448–463
45 Zhang J, Li CM. *Chem Soc Rev*, 2012, 41: 7016–7031
46 Moniz SJA, Shevlin SA, Martin DJ, Guo ZX, Tang J. *Energy Environ Sci*, 2015, 8: 731–759